International Journal of Nanomedicine

Dovepress
Taylor & Francis Group

Open Access Full Text Article

ORIGINAL RESEARCH

Intranasal Delivery of Curcumin-Loaded Pure Drug Self-Assembled Lipid-Based Nanoparticles for Targeted Therapy of Depression

Tao Chen[1,*], Xingyu Liu[2,*], Dandan Li[1], Zhichan Cheng[1], Xi Zheng[1], Zhijie Yu[1]

[1]Pharmacy Department, Chongqing Emergency Medical Center, Chongqing University Central Hospital, Chongqing, 400014, People's Republic of China; [2]Department of Pharmacy, Yibin Maternity and Child Health Care Hospital, Yibin, Sichuan, People's Republic of China

*These authors contributed equally to this work

Correspondence: Zhijie Yu, Department of Pharmacy, Chongqing Emergency Medical Center, Chongqing University Central Hospital, 1 Jiankang Road, Yuzhong District, Chongqing, 400014, People's Republic of China, Email yzj246810@126.com

Purpose: Current antidepressants are limited by insufficient efficacy of conventional monoaminergic drugs and poor brain penetration across the blood-brain barrier. This study designed pure curcumin loaded lipid nanoparticle (CNP) with optimized brain-targeting delivery for depression therapy.

Methods: Cur molecules first self-assembled into carrier-free drug nanoparticles. Subsequently, CNP were then prepared via thin-film dispersion and fully characterized in terms of particle size, PDI, DSC, XRD, TEM. The antidepressant effect of CNP was systematically investigated via in vitro and in vivo assays, including cellular uptake, LPS-induced stress model in BV2 cells, and in vivo CUMS depression model.

Results: CNP displayed uniform spherical morphology with an average size of 115.8 ± 18.3 nm, PDI of 0.216 ± 0.015 and zeta potential of −27.1 mV, along with high encapsulation efficiency (86.11 ± 4.28%), drug loading (6.62 ± 0.45%) and sustained release behavior. The cellular uptake efficiency of the CNP group reached 41.47 ± 1.45%, which was more than double that of the Cur group (17.21 ± 0.54%). In vitro studies showed that CNP not only rescued the viability of cells damaged by corticosterone and hydrogen peroxide but also exerted significantly enhanced anti-inflammatory and antioxidant effects in lipopolysaccharide induced cellular stress models. In vivo studies indicated that CNP alleviated depressive-like behaviors more effectively.

Conclusion: CNP exhibits significantly enhanced antidepressant efficacy, thus providing a promising approach for developing brain-targeted therapeutics for MDD.

Keywords: depression, curcumin, intranasal delivery, self-assembly, drug delivery

Introduction

Major depressive disorder (MDD), also referred to as depression, is a mood disorder whose hallmark feature is loss of interest or sadness for a period of at least two weeks.[1,2] Traditional antidepressants targeting monoaminergic systems exhibit substantial limitations in clinical practice, including a relatively high non-response rate in patients and, in certain instances, the elusiveness of effective symptom improvement with these agents. Furthermore, the adverse effects linked to these agents, such as weight gain and cardiovascular complications, are also notably prominent.[3,4] Ketamine, a novel rapid-acting antidepressant with the ability to restore neuroplasticity, can induce symptom relief in patients with MDD within hours. However, its therapeutic effect exhibits a relatively short duration, and frequent injections are necessitated to maintain efficacy in clinical practice. This not only increases the complexity of treatment procedures but also may raise the risk of drug dependence and adverse reactions.[5,6] As a result, there is a significant gap between the number of MDD patients in need of treatment and the capacity to deliver effective therapy for disease remission.[7,8] The development of new therapeutic agents for MDD is therefore an urgent priority in current clinical and research fields.

https://doi.org/10.2147/IJN.S611765
Received: 27 March 2026
Accepted: 5 June 2026
Published: 12 June 2026

Bioactive phytochemicals exert therapeutic effects via multiple pathways and targets, and have emerged as a promising natural source for the prevention, alleviation, and treatment of depression.[9–11] Curcumin (Cur), a natural polyphenolic bioactive compound, exhibits neuroprotective, anti-inflammatory, and antioxidant properties. Cur can alleviate depressive symptoms by increasing the concentrations of monoamine neurotransmitters in synapses, alleviating dysfunction of the hypothalamic-pituitary-adrenal (HPA) axis, mitigating impairments in neuroplasticity, and counteracting oxidative stress and associated inflammatory dysregulation.[12,13] Currently, curcumin has been proposed as an adjunctive agent for the treatment of depression, curcumin showed strong performance as either monotherapies or adjuncts to antidepressants.[14] Meanwhile, accumulating evidence from clinical randomized controlled trials has demonstrated that Cur serves as an effective therapeutic agent for MDD, and it is well tolerated at high doses with a safety profile comparable to that of placebo.[15,16] As an antioxidant, Cur prevents the elevation of oxidative stress by lowering concentrations of malondialdehyde and protein carbonyls, and enhances the activity of antioxidant enzymes, including superoxide dismutase, catalase, and glutathione peroxidase.[17] Additionally, Cur can modulate synaptic and neuroplasticity-related changes in patients with MDD, including regulating hippocampal levels of BDNF, TrkB, and their downstream factors (ERK, mTOR, and Akt), as well as the expression of components of the cAMP-CREB-BDNF signaling pathway and synapse-associated proteins (Limk1, miR-134, PSD-95, and synapsin).[18,19] However, despite the well-established antidepressant efficacy of Cur, its clinical application is still hindered by several factors, including poor aqueous solubility, low oral bioavailability, rapid metabolism, and rapid systemic clearance.[20]

The emergence of nanomedicines formed via the self-assembly of free drugs or bioactive molecules offers a viable solution to these challenges. Carrier-free nanomedicines constructed through pure drug self-assembly have gained considerable attention due to their high biocompatibility, simple composition, ease of synthesis, and enhanced therapeutic efficacy.[21,22] Pure drug nanoparticles represent a novel class of pharmaceutical formulations formed by the self-assembly of drug molecules in the absence of exogenous carriers.[23,24] Benefiting from their simplified components, more environmentally benign preparation processes, and straightforward manufacturing procedures, these nanoparticles support subsequent large-scale manufacturing and clinical translation. They exhibit key characteristics including small particle size, facile penetration across various biological barriers, and efficient drug release. The nanoscale dimension and uniform physicochemical properties of carrier-free nanomedicines confer enhanced aqueous solubility, improved chemical stability, extended in vivo blood circulation, and strengthened cellular penetration.[25–27] Inspired by the natural multivalent effect, the self-assembly of Cur molecules into carrier-free pure Cur nanoparticles represents a potential strategy to overcome the aforementioned limitations of free Cur.[28] In fact, existing studies have confirmed that Cur can form pure Cur nanomedicines via spontaneous self-assembly.[29] However, carrier-free nanomedicines typically exhibit inadequate targeting capability and face obstacles posed by the blood-brain barrier (BBB).[30,31] Recent studies have demonstrated that coating carrier-free self-assembled drug nanoparticles with phospholipid bilayers can enhance their cellular internalization and modulate intracellular processing.[32] Meanwhile, for drugs like Cur which are characterized by low lipid solubility and limited stability, further improving their brain delivery efficiency is of particular importance for translating their antidepressant potential into clinical utility.

Intranasal administration, a non-invasive drug delivery approach, represents a potential targeted delivery method for brain disorders. Beyond its non-invasive and painless nature, this route can also enhance nasal drug absorption.[33–35] Intranasal administration enables direct drug delivery to the brain via the nose-to-brain pathway, bypassing first-pass metabolism in the liver and intestines to achieve superior therapeutic efficacy. Currently, esketamine (Spravato®), approved by the FDA for intranasal administration, can rapidly alleviate depressive symptoms, and this finding confirms the clinical value of drug delivery through this route.[36] Meanwhile, to address the inherent limitations of Cur in brain delivery, a range of nanomaterial-based encapsulation strategies have been developed, such as polymeric nanoparticles, liposomes, solid lipid nanoparticles, micelles, dendrimers, and hybrid nanomaterials.[21,37] These formulations are designed to enhance curcumin's solubility, stability, cellular internalization, and controlled release, thereby improving its targeted delivery efficiency.[38,39] Among the nanocarriers developed for Cur to date, lipid-based nanocarriers stand out as one of the most extensively investigated systems. In a lipopolysaccharide-induced depressive rat model, curcumin-loaded nanostructured lipid carriers effectively enhanced curcumin's neuroprotective effects, supporting their potential as a therapeutic option for MDD and anxiety.[39,40] Additionally, carrier modification can further boost the efficiency of

brain-targeted delivery. Borneol (Bor), a highly lipid-soluble bicyclic monoterpene, can enhance the ability of drugs to cross biological barriers and serves as a promising brain-targeting auxiliary ligand.[41–43] Studies have leveraged Bor's capacity to improve BBB penetration to successfully deliver the Chinese medicinal monomer Danshen to brain regions, significantly enhancing therapeutic outcomes.[44] In summary, nanodelivery systems can overcome the barrier posed by the BBB that restricts drug delivery to the central nervous system (CNS), improve drugs' brain-targeting capability, and offer potential therapeutic strategies for CNS disorders.[45,46]

In this study, Cur first self-assembled into carrier-free pure curcumin nanoparticles. Subsequently, these nanoparticles were co-encapsulated with Bor, DSPE-mPEG2000, and HSPC to form lipid-based Cur nanoparticles (CNP). With intranasal administration and under the guidance of Bor, CNP can efficiently penetrate into targeted brain regions. This simple lipid-based nanoparticle composed of pure drug combines the non-invasive nature of intranasal administration with brain-targeting capability, thereby offering a promising strategy for accelerating the clinical translation of brain-targeted drug delivery systems for MDD treatment.

Materials and Methods

Materials

Curcumin (Cur, PG77400, 25 g) and Fluoxetine (Flu, P272750, 25 g) were purchased from Chengdu Best Reagent Co., Ltd (China). Corticosterone (CORT, C104537, 1g), hydrogen peroxide (H_2O_2, H755825, 100 mL), HSPC (H304974, 10 g), and DSPE-mPEG2000 (D163634, 10 g) were purchased from were purchased from Aladdin-Reagent Co. Ltd. Cell Counting Kit-8 (CCK-8, CA1210, 500T) were purchased from Beijing Solarbio Science & Technology Co., Ltd (China). NO detection kit (S0021S, 500T) and ROS detection kit (S0033S, >100T) were purchased from Beyotime Biotech Inc. All other chemicals were of chromatographic grade.

Cell Lines and Cultures

BV2 cells and differentiated PC12 cells were obtained from the Basic Medicine Laboratory of the Affiliated Hospital of Southwest Medical University (Sichuan, China). All cell lines were maintained in DMEM (Gibco; Thermo Fisher Scientific, USA) with 10% fetal bovine serum (Hyclone, Utah, USA) and 100 U/mL penicillin-streptomycin in a humidified environment with 5% CO2 at 37 °C.

Preparation and Characterization of CNP

Preparation of CNP

Self-assembled pure Cur nanoparticles were prepared with slight modifications according to previously reported protocols.[28] Briefly, free Cur (5 mg) was dissolved in ethanol (2 mL) and was then rapidly added dropwise to water (10 mL) under vigorous stirring. As solvent exchange occurred and drug molecules self-assembled, the solution gradually turned yellow. Subsequently, the resulting self-assembled pure curcumin nanoparticles were purified and concentrated by dialysis with a dialysis bag followed by centrifugation.

CNP was prepared via the thin film dispersion method, following the specific protocol outlined below. First, 5 mg of self-assembled pure curcumin nanoparticles, 5 mg of Bor, 20 mg of HSPC, and 20 mg of DSPE-mPEG2000 were dissolved in 3 mL of tetrahydrofuran, and the mixture was transferred to a 50 mL round-bottom flask. The mixture was stirred at 100 rpm for 30 min in a constant-temperature water bath at 40 °C. Subsequently, the mixture was moved to a rotary evaporator, and vacuum rotary evaporation was conducted at 40 °C and 100 rpm for 5 min to remove the solvent, leading to the formation of a lipid film on the inner wall of the flask. Nitrogen gas was purged to ensure the absence of residual solvent, and the flask was then placed in a 60 °C oven for approximately 2 h to dry. Subsequently, distilled water was added for hydration, and an ultrasonic cell disruptor (160 W, 5 min) was employed to achieve uniform dispersion of the nanoparticles, which yielded a clear yellow CNP solution. For long-term storage, the CNP solution was pre-frozen in a −80 °C freezer, followed by freeze-drying (using a freeze dryer) for approximately 24 h, ultimately yielding a clear yellow, loose CNP lyophilized powder.

Characterization of CNP

Particle size, polydispersity index (PDI), and zeta potential of CNP were measured using a Malvern laser particle size analyzer. Briefly, the prepared CNP lyophilized powder was dissolved and diluted to a suitable concentration; the resulting solution was then transferred to a 1 mL sample cell. Measurements were performed by injecting the sample into the analyzer and conducted at room temperature (25 °C). Calorimetric analysis was conducted using a differential scanning calorimeter (DSC, Model DSC 214 Polyma; NETZSCH). Under a nitrogen atmosphere, an aluminum pan loaded with an appropriate amount of sample was heated from 50 °C to 300 °C at a rate of 10 °C/min, and the DSC curve was generated from the scanning data. Wide-angle X-ray diffraction (XRD) analysis was performed using an X-ray diffractometer (Model Bruker D8 ADVANCE; Bruker Corporation) with scanning from 5° to 80° at a rate of 6°/min under operating conditions of 40 kV and 30 mA. Transmission electron microscopy (TEM) was employed to characterize the morphological characteristics of CNP. Briefly, the CNP sample solution (reconstituted in water) was deposited onto a copper grid, then negatively stained with 1% (w/v) sodium phosphotungstate. Subsequently, the grid was imaged using a TEM to acquire images of CNP morphology.

Encapsulation Efficiency and Loading Efficiency

An equal mass (10 mg each) of CNP lyophilized powder and bulk Cur was accurately weighed. To facilitate the complete release and dissolution of encapsulated Cur from the nanoparticles, 5 mL of methanol was added to each sample. After ultrasonication for 4 min, the mixtures were appropriately diluted to prepare a CNP lipid nanoparticle solution and a bulk Cur solution. Both solutions were then transferred to a centrifuge and centrifuged at 8000 rpm for 10 min. The Cur content in each supernatant was quantified via high-performance liquid chromatography (HPLC). The Cur concentration in the CNP lipid nanoparticle solution was designated as C1, and that in the bulk Cur solution as C2. The encapsulation efficiency (EE) of CNP was calculated using the formula below.

$$\mathrm{EE}(\%) = \mathrm{C1}/\mathrm{C2} \times 100\%$$

Separately, 10 mg of CNP lyophilized powder was accurately weighed (designated as W) and completely dissolved in a fixed volume of pure water. To facilitate the release of Cur encapsulated in the lipid nanoparticles, 5 mL of methanol was added to the resulting solution. After 4 min of ultrasonication, the mixture was appropriately diluted, and centrifugation was then performed at 8000 rpm for 10 min. The Cur content in the supernatant was quantified via HPLC. The measured value was substituted into the pre-established standard curve to calculate the exact amount of Cur in W grams of the lyophilized powder, which was designated as W1. The loading efficiency (LE) of CNP was calculated using the formula below.

$$\mathrm{LE}(\%) = \mathrm{W1}/\mathrm{W} \times 100\%$$

In vitro Release

The in vitro release study was conducted via the dialysis method using an intelligent dissolution tester (ZRS-8G; Tianjin Tianda Tianfa Technology Co., Ltd., Tianjin, China). A total volume of 120 mL phosphate-buffered saline (PBS, pH 6.5) was used as the release medium to evaluate the in vitro release behavior of CNP. Given the poor aqueous solubility of free Cur, an appropriate amount of surfactant (0.2% Tween 80) was added to the release medium. Dialysis bags were each loaded with 2 mL of either CNP solution (1 mg/mL) or free Cur solution, with both solutions having the same Cur concentration. The release medium was maintained at 37 ± 0.5 °C under continuous stirring at 100 rpm. At preset time points 0 h, 0.25 h, 0.5 h, 1 h, 2 h, 4 h, 8 h, 12 h and 24 h, 2 mL of dialysate was withdrawn, and an equal volume of fresh release medium was replenished to maintain a constant total volume. Following centrifugation of the collected dialysate, the Cur concentration was quantified via ultraviolet-visible (UV-Vis) spectroscopy. For each in vitro release experiment, all collected samples were analyzed in triplicate using UV-Vis spectroscopy. The cumulative release percentage at each time point was calculated using the pre-established standard curve, and the in vitro release profile was then plotted.

Stability

To investigate the long-term storage stability of CNP freeze-dried powder, the powder was stored in a 4 °C refrigerator. Samples were collected at eight key time points during storage, including days 3, 5, 7, 14, 30, 60, 120 and 180. Particle size, PDI and zeta potential were determined to evaluate changes associated with storage. All tests were performed at room temperature. Three parallel samples were randomly selected at each time point. After redissolution, the samples were vortexed thoroughly and allowed to stand for 5 minutes to ensure uniform dispersion.

In vitro Hemolytic Analysis

To evaluate the in vivo biosafety of CNP during systemic circulation, a hemolysis assay was performed. For animal blood collection, fresh blood was collected from the retro-orbital venous plexus of mice. Anesthesia is first administered by placing mice in a closed container for nasal inhalation of isoflurane at a flow rate of 1.0 L/min. Three minutes after the mice inhale isoflurane, 0.3 mL of blood is collected using the inner canthus blood collection method. Immediately after blood collection is completed, the mice are placed back into the closed container and administered a high concentration of isoflurane at a flow rate of 2.0 L/min for euthanasia via excessive anesthesia. The interval between blood collection and the re-administration of high-concentration isoflurane for mouse euthanasia is less than 1 min. The collected blood was transferred to anticoagulant-containing test tubes to prevent coagulation. The blood samples were gently stirred with a glass rod for 5 min to inhibit fibrinogen-mediated coagulation. Subsequently, an appropriate volume of 0.9% normal saline was added; after gentle mixing, the mixture was centrifuged at 1500 rpm for 10 min, and the supernatant was carefully removed. To isolate pure red blood cells (RBCs), normal saline was added to the pellet, and this stirring and centrifugation cycle was repeated until the supernatant became completely colorless. The washed RBCs were resuspended in normal saline to prepare a 2% RBC suspension, which was stored for subsequent use. CNP solutions at different concentrations (25 μg/mL, 50 μg/mL, 75 μg/mL, 100 μg/mL) were mixed with the 2% RBC suspension, alongside two control groups: a negative control (normal saline) and a positive control (ultrapure water). All mixtures were incubated in a 37 °C incubator to induce hemolysis. After 5 h of static incubation, all samples were centrifuged at 1500 rpm for 10 min, and the supernatant was collected to assess the hemolysis degree of each group. The supernatant from each group was aspirated and transferred to a 96-well microplate. A microplate reader was used to measure the absorbance (denoted as A) of each well at a wavelength of 540 nm, and the hemolysis percentage (%) of each group was further calculated based on the absorbance data.

Cytotoxicity Study

A CCK-8 assay was employed to evaluate the effects of CNP at different concentrations on the viability of PC12 cells and BV2 cells. PC12 cells and BV2 cells were first resuscitated in high-glucose DMEM supplemented with 10% fetal bovine serum. The resuscitated cells were transferred to a cell incubator for stationary culture, and the medium was refreshed periodically to maintain optimal cell growth. When the cells reached the logarithmic growth phase, they were digested with 0.25% trypsin-EDTA. After adjusting the cell concentration, the cells were seeded into 96-well plates with a strict seeding density of 5000 cells per well in 100 μL of medium. The seeded 96-well plate was placed in the incubator. Following 24 h of cell adhesion and growth, drug treatment was initiated: 100 μL of CNP solutions at gradient concentrations (10 μg/mL, 7.5 μg/mL, 5 μg/mL, 2.5 μg/mL, 1 μg/mL) was added to each experimental well, while the blank control group received an equal volume of drug-free high-glucose DMEM. The treated 96-well plate was returned to the incubator for an additional 24 h of culture. After this period, 10 μL of CCK-8 reagent was added to each well. The plate was gently shaken to ensure thorough mixing before being placed back in the incubator for another 4 h of incubation, allowing adequate reaction between the reagent and viable cells. At the end of incubation, a microplate reader was used to measure the absorbance of each well at a wavelength of 450 nm. Cell viability was calculated from these absorbance values, and the effects of CNP at different concentrations on the viability of the two cell lines were further analyzed.

Cellular Uptake

Fluorescence microscopy was used to visually assess the uptake of CNP by BV2 cells. Cur exhibits intrinsic fluorescence, and this property enables tracking of CNP cellular uptake without additional labeling. The specific protocol was as

follows: BV2 cells in the logarithmic growth phase were seeded into 6-well plates at a density of 3×10^5 cells per well. Each well received 2 mL of complete culture medium, and the plates were incubated to allow 24 h of adherent growth—ensuring sufficient cell attachment and adaptation to the culture environment. Three experimental groups were established: a blank control group (100 μL of drug-free basal medium), CNP experimental groups at gradient concentrations, and Cur control groups at corresponding concentrations. For drug-treated groups, 100 μL of culture medium containing the respective drug (1 μg/mL, 5 μg/mL, 10 μg/mL) was added. After incubation for 2 h or 4 h, the culture medium in each well was gently aspirated and removed. Cells were rinsed three times with PBS (pH 7.4) to completely eliminate residual free drug, which prevented interference with fluorescence imaging. Subsequently, an inverted fluorescence microscope was used to observe intracellular fluorescence distribution, and images were acquired using the Olympus UC90 color imaging system to document differences in CNP uptake by cells across different time points and concentrations. To quantify the cellular uptake of CNP, HPLC was employed for detection. BV2 cells were seeded in 6-well plates and allowed 24 h of adherent growth, then treated with CNP for 4 h. Cells were harvested via scraping with a cell scraper, followed by centrifugation at 800 rpm for 5 min to collect the cell pellet. Cell lysis buffer supplemented with a protease inhibitor cocktail was added, and cells were lysed on ice for 30 min. Four volumes of methanol were added to precipitate proteins and extract CNP, followed by high-speed centrifugation (12,000 rpm, 4 °C) for 15 min. The supernatant was filtered through a 0.22 μm organic-phase filter membrane, and the CNP content in the filtrate was quantified using an HPLC system to further calculate the cellular uptake efficiency.

Evaluation of H_2O_2-Induced PC12 Cell Injury Model

PC12 cells in the logarithmic growth phase were collected and seeded into 96-well plates at a density of 5000 cells per well. Each well received 100 μL of high-glucose DMEM complete medium supplemented with 10% fetal bovine serum, and the plates were placed in a cell incubator for culture. Following 24 h of cell adhesion and growth, four experimental groups were established with 3 technical replicates per group: the blank control group received 100 μL of drug- and H_2O_2 -free complete medium per well; the H_2O_2 model group received 100 μL of complete medium containing a predetermined concentration of H_2O_2 per well to induce a cellular injury model; the gradient concentration CNP intervention groups and Cur intervention groups each received 100 μL of complete medium supplemented with both the respective drug (1 μg/mL, 5 μg/mL, 10 μg/mL) and H_2O_2 per well. The 96-well plate was returned to the incubator for an additional 24 h of culture. After this period, 10 μL of CCK-8 reagent was added to each well. The plate was gently shaken to ensure uniform reagent distribution before being placed back in the incubator for another 4 h of incubation. At the end of incubation, a microplate reader was used to measure the absorbance (A value) of each well at 450 nm. With the absorbance of the blank control group as the reference, the relative cell proliferation rate was calculated to evaluate the effects of different drug concentrations on the viability of H_2O_2-injured PC12 cells.

Evaluation of CORT-Induced PC12 Cell Injury Model

The CORT-induced PC12 cell injury model was established using a protocol similar to that of the H_2O_2-induced model. PC12 cells in the logarithmic growth phase were collected and seeded into 96-well plates at a density of 5000 cells per well. Each well received 100 μL of high-glucose DMEM complete medium supplemented with 10% fetal bovine serum, and the plates were placed in a cell incubator for culture. Following 24 h of cell adhesion and growth, four experimental groups were established with 3 technical replicates per group: the blank control group received 100 μL of drug- and CORT-free complete medium per well; the CORT model group received 100 μL of complete medium containing a predetermined concentration of CORT per well to induce a cellular injury model; the gradient concentration CNP intervention groups and Cur intervention groups each received 100 μL of complete medium supplemented with both the respective drug (1 μg/mL, 5 μg/mL, 10 μg/mL) and CORT per well. The 96-well plate was returned to the incubator for an additional 24 h of culture. After this period, 10 μL of CCK-8 reagent was added to each well. The plate was gently shaken to ensure uniform reagent distribution before being placed back in the incubator for another 4 h of incubation. At the end of incubation, a microplate reader was used to measure the absorbance (A value) of each well at 450 nm. With the absorbance of the blank control group as the reference, the relative cell proliferation rate was calculated to evaluate the effects of different drug concentrations on the viability of CORT-injured PC12 cells.

Stress Model of BV2 Cells Induced by LPS

BV2 cells in the mid-logarithmic growth phase were seeded into 6-well plates and incubated for 24 h under optimal culture conditions. After cells had adhered and achieved good growth, the original medium was replaced with high-glucose DMEM containing Cur at three concentrations (1 μg/mL, 5 μg/mL, 10 μg/mL) mixed with lipopolysaccharide (LPS), with 3 technical replicates per group. Following 12 h of drug treatment, culture supernatants were collected after centrifugation in strict accordance with the standard protocol provided in the NO detection kit instructions. A predetermined volume of NO detection reagent was added; after sufficient reaction, a microplate reader was used to quantify NO levels in each group at the specified wavelength. Relative NO content in each group was calculated with reference to the blank control group.

The grouping and drug treatment protocols for the ROS assay were identical to those for the NO assay. After 12 h of treatment, culture supernatants were carefully aspirated, and cells were rinsed three times with pre-chilled PBS to remove residual medium components. Subsequently, an appropriate volume of ROS detection reagent was added following the detailed procedures outlined in the ROS detection kit instructions. After sufficient reaction, intracellular staining patterns were first observed under an inverted fluorescence microscope, and then a microplate reader was used to measure fluorescence intensity in each group. Relative ROS fluorescence intensity was calculated for each group, with results expressed as relative fluorescence intensity and the blank control group assigned a value of 100%.

In vivo Antidepressant Effect of CNP

Experimental animals: Male C57BL/6J mice (7 weeks old, body weight 18 ± 2 g) were purchased from Sibeifu (Beijing) Biology Technology Co., Ltd. All mice were housed in a specific pathogen-free (SPF) grade environment with a 12 h light/dark cycle. The housing conditions were controlled at a temperature of 22 ± 2°C and a relative humidity of 50 ± 10%. Mice had free access to standard feed and drinking water. A 1-week acclimation period was provided before the experiment to allow mice to adapt to the housing environment. All animal experiments were approved by the Ethics Committee of Chongqing University Central Hospital (NO.2502002) and performed in strict accordance with the Guide for the Care and Use of Laboratory Animals.

Establishment of chronic unpredictable mild stress (CUMS)-induced depression model: After acclimation to the environment mice were randomly divided into a blank control group and a CUMS model group. The CUMS depression model was established using a combination of multiple unpredictable mild stressors with a stress cycle of 42 days. The specific stressors included ice water swimming 24 h food deprivation 24 h water deprivation vigorous cage shaking for 10 min centrifuge tube restraint for 2 h continuous light for 24 h continuous darkness for 24 h and noise stimulation for 2 h among others. Two different stressors were administered daily without repeating the same stressor to maintain the unpredictability of stress.

Grouping and administration: After successful establishment of the CUMS model all mice were further divided into 5 groups (n = 6 per group). The grouping and administration protocol were as follows. The blank control group received intranasal normal saline. The CUMS model group received an equal volume of normal saline via intranasal administration. The fluoxetine (positive control) group was given fluoxetine at 10 mg/kg via intragastric gavage. The low-dose CNP group received CNP at 10 mg/kg via intranasal administration. The high-dose CNP group was administered CNP at 20 mg/kg via intranasal route. The doses of fluoxetine and CNP were selected based on previously published antidepressant studies in mice and further justified by body surface area-based dose translation from mice to humans.[16,28,47] Fluoxetine at a dose of 10 mg/kg is a classic and widely used positive control dose in mice CUMS depression models. According to the body surface area conversion method, the mouse doses of 10–20 mg/kg correspond to approximately 0.81–1.62 mg/kg in humans (conversion factor = 1/12.3), which is within a reasonable and safe range for potential clinical application. The dosage of CNP (10 mg/kg, 20 mg/kg, calculated as curcumin) refers to the reported dosage of curcumin in vivo to ensure that the administration is effective and non-toxic. All drugs and normal saline were administered once daily for 28 consecutive days. Normal saline and drug formulations were freshly prepared before each administration to ensure their stability.

Depressive-like behavior tests: After 28 days of administration three behavioral tests were conducted to evaluate depressive-like phenotypes in mice including open field test (OFT) forced swim test (FST) and sucrose preference test (SPT). All behavioral tests were performed during the light phase of the circadian rhythm with the test environment kept quiet. After each mouse completed the test the test apparatus was thoroughly cleaned with 75% ethanol to eliminate residual olfactory cues and prevent interference with subsequent test results.

Animal euthanasia protocol: Mice were placed in a closed container and anesthetized with high-concentration isoflurane delivered at a flow rate of 2.0 L/min. Continuous administration of isoflurane induced respiratory depression. Following the loss of consciousness in mice, the isoflurane concentration was maintained at 5% for approximately 15 min. Euthanasia was confirmed by the cessation of breathing and heartbeat, loss of pupillary reflex, and absence of hind limb withdrawal response when the hind limb toes were pinched with tweezers.

Statistical Analysis

All data were analyzed using GraphPad Prism 10.1.2 software. Data are expressed as mean ± standard deviation (SD), and were based on three independent experimental replicates. For statistical analysis, Student's *t*-test was used to compare differences between two groups, while one-way analysis of variance (ANOVA) followed by a post-hoc test was employed for comparisons among multiple groups. Statistical significance was defined as $P < 0.05$.

Results

Characterization of CNP

The development of pure drug nanoparticles, formed by the self-assembly of free drugs or bioactive molecules, has garnered considerable attention due to their high drug-loading capacity, straightforward preparation protocols, and nature as an "integrated" functional platform. Pure drug nanoparticles, however, exhibit intrinsic instability to some extent. Such instability renders them susceptible to premature drug release or aggregation in the complex physiological microenvironment; this, in turn, results in their rapid clearance and diminished therapeutic efficacy.[22,26] To enhance the stability and biocompatibility of pure drug nanoparticles, we encapsulated the drugs by means of lipid-based carriers. However, nanomedicines exhibit inadequate targeting capability and face obstacles posed by membrane barriers, including the blood-brain barrier. Thus, we incorporated borneol into the drug delivery system to modify it, aiming to enhance the brain delivery efficiency of the test drug. The raw materials required for this nanoparticle are commercially available and low-cost, with a simple and controllable preparation process, showing great potential for subsequent scale-up production and favorable cost-effectiveness. In this study, we successfully prepared the targeted drug delivery system CNP, as illustrated in Figure 1A. The CNP solution exhibits an orange-yellow color and yields an orange-yellow powder after lyophilization, a hue consistent with that of curcumin powder. Subsequently, to confirm that CNP possessed an appropriate particle size, we conducted relevant characterization of CNP with a Malvern laser particle size analyzer. As shown in Figure 1B, CNP displayed an average particle size of 115.8 ± 18.3 nm and a PDI of 0.216 ± 0.015, indicating it possesses an appropriate particle size and excellent dispersive uniformity. Nanoparticles tend to aggregate spontaneously. Notably, a high zeta potential, regardless of being positive or negative, indicates strong electrostatic repulsion between individual particles, thereby bolstering their stability. An appropriate zeta potential enables nanoparticles to maintain stable dispersibility for an extended period. In the range of 5–30 mV, nanoparticles exhibit limited flocculation or only short-term stability. In contrast, a zeta potential below 5 mV usually leads in particle aggregation.[48] As shown in Figure 1C, the zeta potential of CNP was measured at −27.1 mV, which indicates excellent electrostatic stability. Subsequently, the UV absorption behavior of CNP was determined. As shown in Figure 1D, full-wavelength scanning was performed on both the bulk drug employed in this study and the targeted formulation CNP. Within the wavelength range of 300–550 nm, the maximum UV absorption of Cur occurred at approximately 428 nm. The UV absorption profile of CNP was essentially consistent with that of Cur, while no UV absorption was detected for excipients at this wavelength. This allows the maximum absorption wavelength to be directly used for detection when establishing the HPLC methodology for drug solubility, thereby laying a solid foundation for the subsequent determination of drug release.

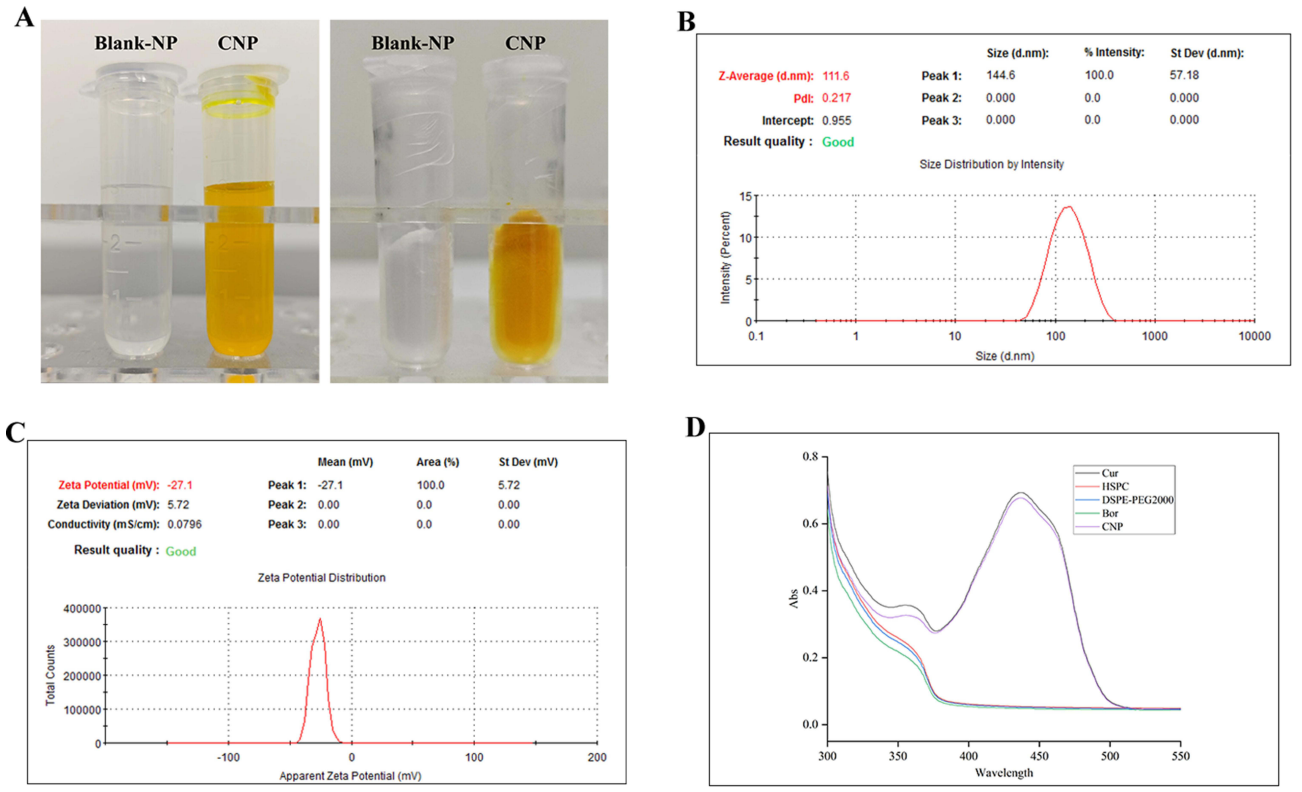

Figure 1 Characterization results of CNP. (**A**) Digital images of blank nanoparticles and CNP (solution and freeze-dried powder). (**B**) Particle size distribution profile of CNP as determined by a Malvern particle size analyzer. (**C**) Zeta potential profile of CNP as determined by a Malvern particle size analyzer. (**D**) UV scanning spectra of CNP and other excipients. ($\bar{x} \pm s$, n = 3).

Morphological Characterization of CNP

DSC analysis (Figure 2A) showed that Cur had a melting point of 184.85 °C, while blank nanoparticles (drug-free) exhibited a glass transition temperature of 58.49 °C. For the CNP group, the characteristic endothermic peak of Cur disappeared, suggesting that drug molecules were successfully encapsulated in the hydrophobic core of lipid-based materials. XRD scanning (Figure 2B) revealed that Cur crystals had multiple signal peaks in the 5°–30° range, with the strongest characteristic signal peak occurring at 20°. In the CNP curve, the characteristic diffraction peaks of Cur were no longer detectable This indicated that Cur had converted to an amorphous state in CNP, thereby further confirming that drug loading was successful. Subsequently, the physical morphology of CNP was further observed directly via TEM. As shown in Figure 2C, CNP exhibited a nanoscale spherical-like morphology, with an approximate particle size of 100 nm and relatively uniform size and distribution. Natural small molecules typically self-assemble spontaneously into stable pure drug nanoparticles via non-covalent intermolecular interactions, including hydrophobic interactions, π-π stacking, hydrogen bonding, electrostatic forces, and coordination interactions.[49] Thus, no new functional groups are generated. However, encapsulation by lipid membranes may mask the characteristic peaks of small molecules. As shown in the FT-IR curve (Figure 2D), Cur exhibits FT-IR characteristic peaks at 1627, 1508 and 1430 cm^{-1}. However, these peaks are largely masked in CNP. Meanwhile, the characteristic peaks of the excipients HSPC and DSPE-mPEG2000 were observed at 2920 and 1115 cm^{-1}. Furthermore, phospholipids are widely acknowledged to possess a unique ability for spontaneous self-assembly in aqueous environments. To reduce edge exposure, lipid segments bend spontaneously to form curved discs. This curvature reduces boundary interaction energy and optimizes system free energy by exposing hydrophilic moieties to water while shielding hydrophobic regions. CNP in this study also exhibited similar morphological characteristics. The size of nanoparticles is a key factor influencing their ability to cross the BBB. Studies have demonstrated that the smaller their size, the greater their ability to permeate the BBB. However, nanoparticles smaller than 5 nm are more prone to filtration and

https://doi.org/10.2147/IJN.S611765

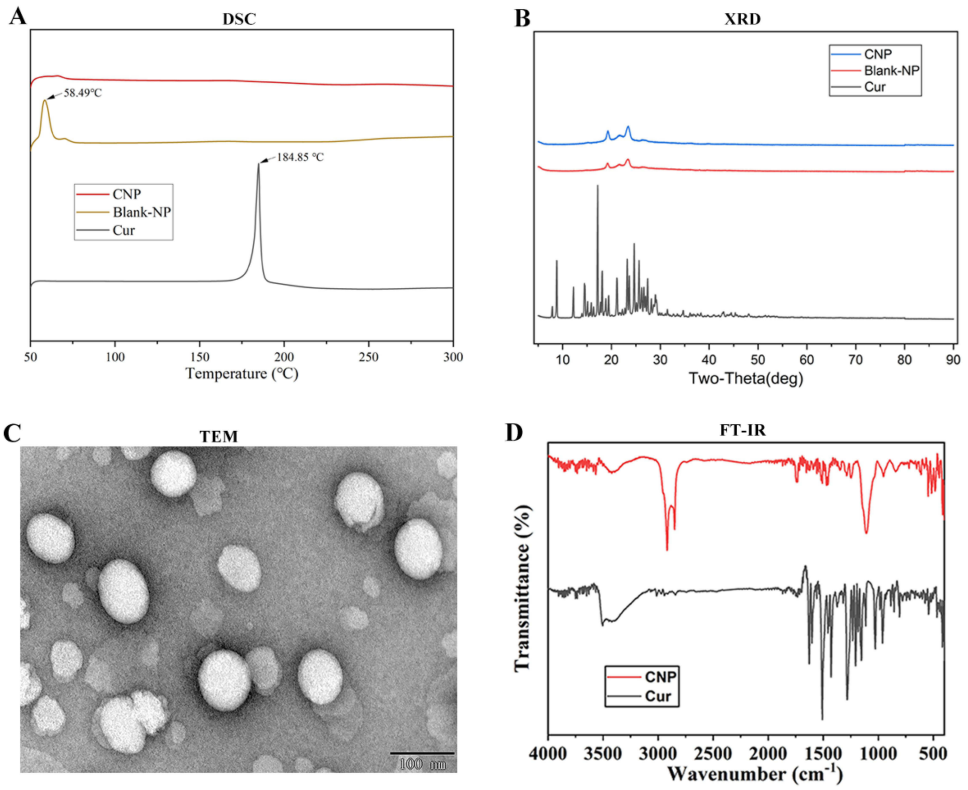

Figure 2 Morphological characterization of CNP. (**A**) DSC thermograms of CNP. (**B**) X-ray diffraction patterns of CNP. (**C**) The TEM images of CNP. (**D**) Fourier transform infrared spectroscopy of CNP.

elimination by the liver, whereas those larger than 200 nm are largely unable to cross the BBB.[50] In this study, CNP had an approximate particle size of 100 nm, indicating it had a relatively suitable size for BBB penetration.

In vitro Release and Stability Study

After successfully preparing CNP, we first determined the LE and EE of the system. As shown in Figure 3A, we established a standard curve for Cur solubility using full-wavelength UV scanning data. Measurements showed that CNP achieved an EE of 86.11% and a LE of 6.62%. Subsequently, we assessed the drug release profile of CNP via the dialysis method. As shown in Figure 3B, Cur exhibited a burst release pattern: at 8 h, its cumulative release rate reached 83.97 ± 2.88%, and it had essentially reached release equilibrium by this time. In contrast, the CNP group showed distinct phase-dependent characteristics of drug release. Specifically, CNP released the drug rapidly in the first 8 h, with a cumulative release rate of 48.76 ± 2.72%; thereafter, a slow-release phase was observed. By 24 h, the cumulative release rate had increased to 65.62 ± 2.43%, confirming that the system exhibited sustained release behavior. The drug release curve shows that CNP exhibits significantly delayed drug release. Typically, pure drug nanoparticles have a relatively fast release rate due to the supramolecular physical properties of self-assembled drugs. However, benefiting from encapsulation within lipid-based carriers and the "stealth" property imparted by PEG chains that form a hydrophilic shell, the systemic circulation time of the nanosystem is significantly prolonged.[51] Accordingly, lipid-based nanomedicines exhibit a biphasic release process. In the initial phase, the drug is released via diffusion from the lipid matrix, a release trend which is similar to that of bulk Cur. In the subsequent phase, as the lipid-based carriers themselves degrade, drug entrapped within the lipid membrane is gradually released. This characteristic further underscores the capacity of lipid-based carriers to facilitate sustained drug release while preventing the oxidation and premature degradation of Cur.

The stability investigation results of CNP are presented in Figure 3C. CNP freeze-dried powder maintained excellent stability at 4 °C (low temperature). Its particle size, PDI and zeta potential remained relatively stable for 120 days. After 180 days of storage, particle size and PDI increased slightly. The absolute value of zeta potential decreased. The

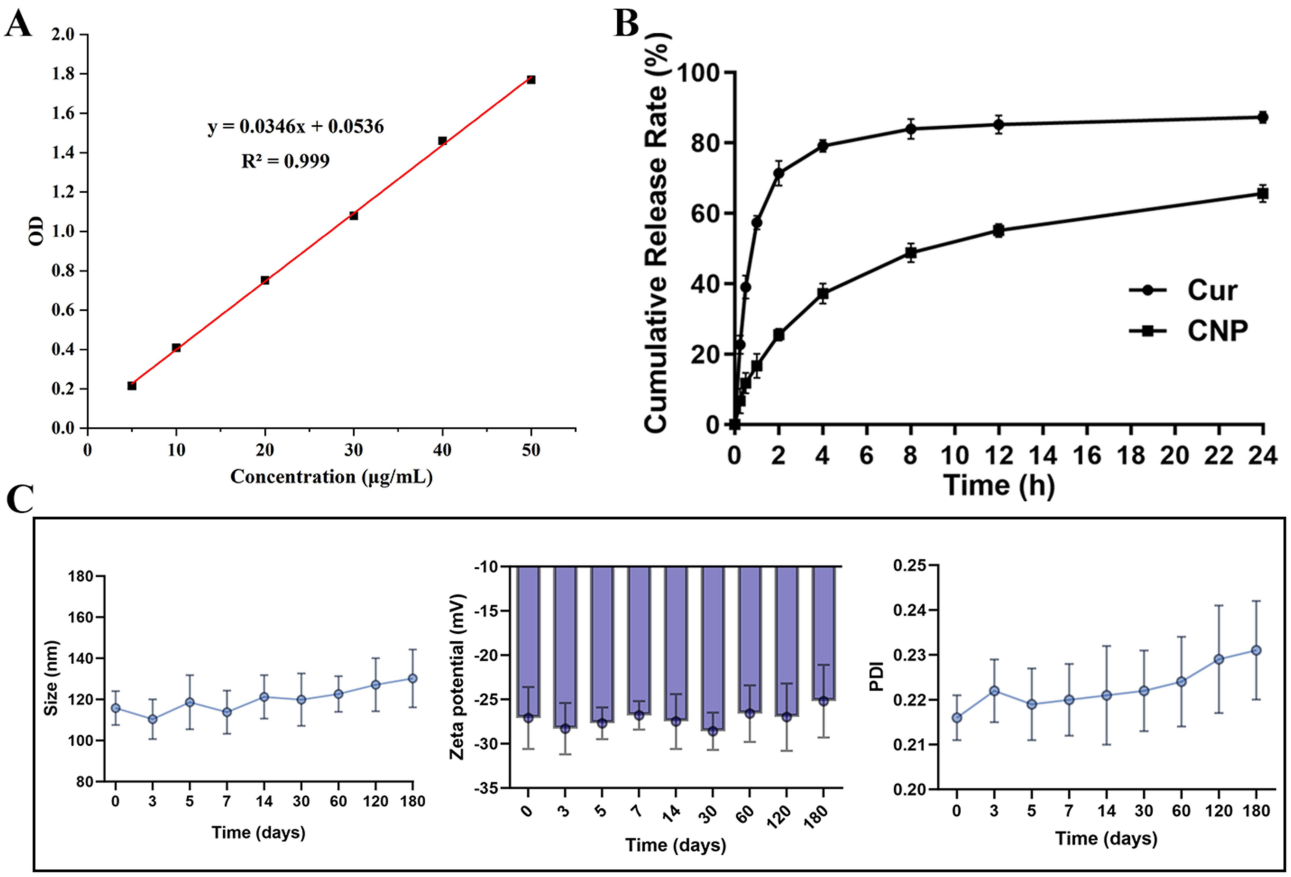

Figure 3 CNP exhibits a capacity for sustained drug release. (**A**) Solubility standard curve of Cur. (**B**) Release profiles of Cur and CNP in PBS release medium (pH 7.4) over 24 h. (**C**) Changes of particle size, PDI and zeta potential (absolute value) of CNP freeze-dried powder stored at room temperature (25 °C) for 180 days. ($\bar{x} \pm s$, n = 3).

nanoparticles still remained within the ideal nanoscale range. They maintained satisfactory stability throughout the storage period. This phenomenon can be explained by the structural characteristics of self-assembled nanoparticles. Self-assembled nanoparticles composed of pure drugs mainly depend on intermolecular non-covalent forces. These forces include intermolecular hydrophobic interactions, π-π stacking and hydrogen bonding. These non-covalent bonds exhibit weak binding affinity. They are susceptible to interference from external factors. After encapsulation with lipid-based carriers, the nanoparticles gain effective protection from lipid bilayers. This protective effect results in significantly enhanced stability compared to pure curcumin self-assemblies.

Cytotoxicity and Biocompatibility

Since this study aimed to deliver CNP to the brain, we first selected PC12 cells and BV2 cells to assess the cytotoxicity of CNP. This selection allowed us to preliminarily evaluate both the cytocompatibility of CNP and its cellular uptake rate, without confounding cytotoxic effects. As shown in Figure 4A and B, within the drug concentration range of 1–10 μg/mL, PC12 cells and BV2 cells maintained a healthy growth state 24 h after treatment with either free Cur or CNP. The relative cell viability of each treatment group exhibited no significant differences compared with the blank control group, which indicates that CNP has good cellular safety. This non-cytotoxic concentration range is ideal for subsequent cellular uptake studies.

Subsequently, the hemolysis rate of CNP was tested. In general, a hemolysis rate of less than 5% is regarded as non-hemolytic, indicating good safety, whereas a rate exceeding this threshold signifies inherent toxicity. As shown in Figure 4C, the negative control group showed a colorless, transparent solution with a hemolysis rate of 0%, whereas the positive control group exhibited a bright red solution with a hemolysis rate of 100%. Four CNP concentration groups were established, with concentrations ranging from 25 to 100 μg/mL. Although the hemolysis rate increased slightly as

https://doi.org/10.2147/IJN.S611765

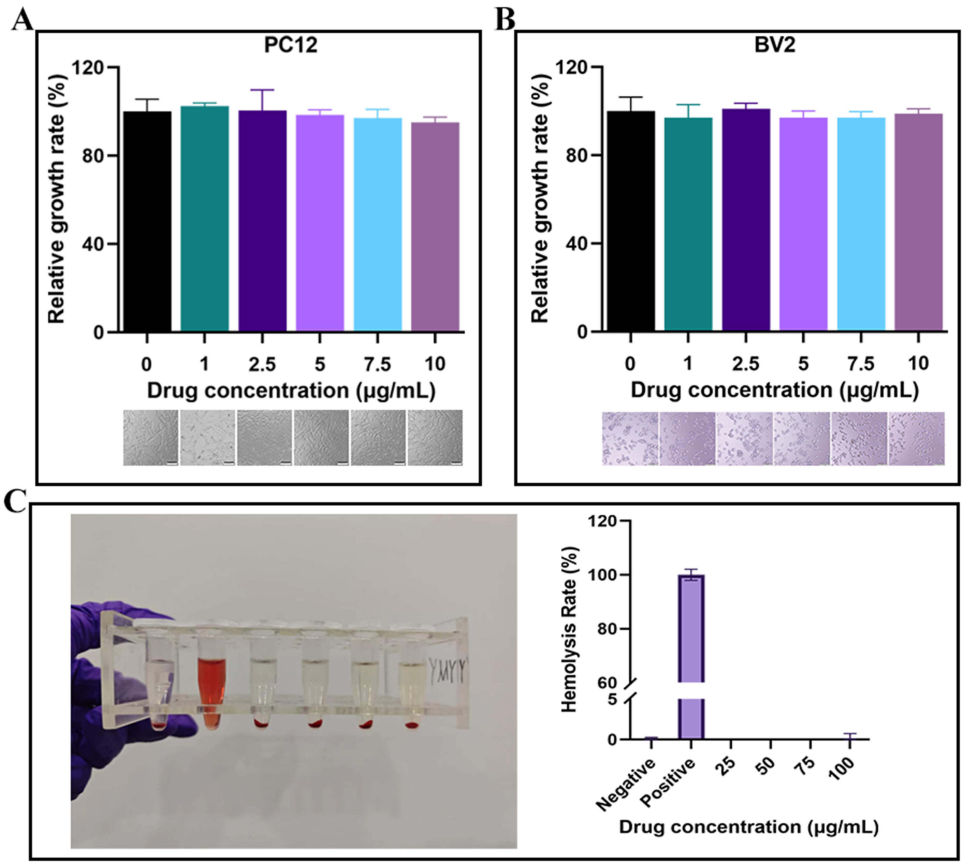

Figure 4 CNP exhibit favorable cellular safety and biocompatibility. (**A**) Effects of CNP at gradient concentrations on the relative growth rate of PC12 cells, and digital images of representative cells at each concentration. (**B**) Effects of CNP at gradient concentrations on the relative growth rate of BV2 cells, and digital images of representative cells at each concentration. (**C**) Quantitative results and digital images of the CNP hemolysis assay at gradient concentrations. ($\bar{x} \pm s$, n = 3).

CNP concentration increased, all values remained far below 5%. At the highest concentration of 100 μg/mL, the maximum hemolysis rate was 0.16 ± 0.6%. This observation may be attributed to electrostatic interactions between the negative charge of CNP and the positively charged phosphocholine lipids on the outer membrane of red blood cells. However, even at the maximum tested concentration of 100 μg/mL, the hemolysis rate remained extremely low, which confirms that CNP nanoparticles possess excellent biocompatibility.

Cellular Uptake

When drugs reach target cells, their intracellular journey begins with cellular uptake, which typically takes place through endocytosis.[51] For many drug delivery systems, the cytoplasm acts as the final destination for the effective payload. Owing to its intrinsic fluorescent properties, Cur enables observation of cellular drug uptake via fluorescence microscopy, eliminating the need for additional fluorescent dyes. As shown in Figure 5A, Cur emits green fluorescence, and following cellular uptake, it localizes predominantly in the cytoplasm. We quantified the cellular uptake rate via HPLC (Figure 5B). Under the same administration concentration and treatment duration, the fluorescence intensity in the CNP group was higher than that in the corresponding free Cur group. Furthermore, when comparing 2 h and 4 h treatment durations, the cellular uptake rate increased with the prolongation of treatment time. At 4 h, the cellular uptake rate of the CNP group reached 41.47 ± 1.45%, which is more than twice the 17.21 ± 0.54% observed in the Cur group. The composition and structure of lipid-based carriers enable the regulation of in vivo drug activity, including biodistribution in specific cells, cellular uptake, the extent of intracellular drug release, and drug functionality.[52] Existing studies have demonstrated that incorporating a phospholipid bilayer into drug-only nanoparticles enhances their cellular uptake and alters their intracellular processing.[32] Additionally, the binding or adsorption of Bor to the cell membrane inhibits P-glycoprotein mediated efflux,

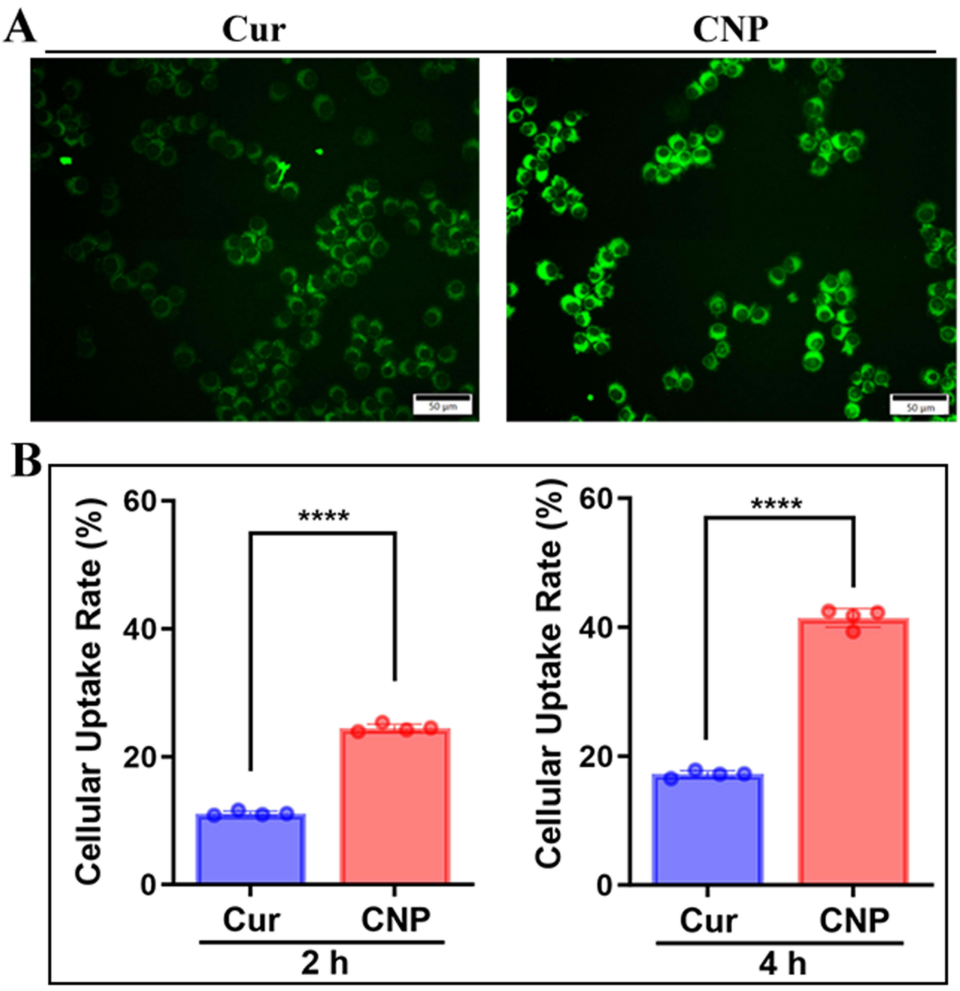

Figure 5 CNP exhibit enhanced uptake efficiency by BV2 cells. (**A**) Digital images of CNP uptake by BV2 cells. (**B**) At the 2nd and 4th hours, the uptake efficiency of BV2 cells for Cur and CNP was determined respectively. ****$P < 0.0001$. ($\bar{x} \pm s$, n = 4).

increases membrane fluidity, and promotes the ordered arrangement of phospholipid molecules.[53] These effects collectively contribute to increased cellular drug uptake and prolonged intracellular drug retention. Notably, prolonged intracellular drug concentration and retention time suggest that the drug may exhibit stronger biological activity.

Neuroprotective Effect

Following the successful preparation and systematic characterization of the physicochemical properties of CNP, we preliminarily evaluated the biological effects of this nanomaterial. The incidence of depression is closely associated with dysfunction of the HPA axis. Notably, patients with depression often exhibit elevated serum cortisol levels. Correspondingly, exogenous administration of high-dose CORT can induce changes in behavior, neurochemistry, and brain anatomy. Separate studies have shown that exposure to an environment with elevated CORT levels can induce depressive-like behaviors in mice. Classic monoaminergic antidepressants, including Flu and imipramine, have been shown to prevent CORT-induced depressive-like behaviors in mice. They also restore abnormal cellular changes in the hippocampus of mice with depressive-like phenotypes.[54,55] Furthermore, the brain has high oxygen consumption and a lipid-rich microenvironment. This makes it highly sensitive to oxidative stress or redox imbalance.[56] Under conditions of oxidative stress, strong oxidants such as H_2O_2 far exceed the brain's clearance capacity. Consequently, high concentrations of these oxidants are frequently detected in patients with depression. Existing studies have demonstrated effective antidepressant effects by reducing H_2O_2 levels and restoring redox homeostasis.[57] Therefore, to investigate

https://doi.org/10.2147/IJN.S611765

whether CNP exhibits cellular protective capacity like or greater than that of Cur, we first evaluated the pharmacodynamic effects of CNP using an established in vitro antidepressant model. This model was primarily made up of two cell injury models. These two models were one induced by CORT and the other by H_2O_2. As shown in Figure 6A, CORT treatment led to a significant reduction in the relative cell growth rate, which decreased to 41.19 ± 0.52%. As CNP was added and its concentration increased, the protective effect of CNP against CORT-induced cell injury gradually enhanced. When the CNP concentration reached 10 μg/mL, the relative cell growth rate was restored to 85.18 ± 0.58%. At all tested concentrations, CNP exhibited stronger biological activity than Cur at the corresponding concentration. This observation may be attributed to two key factors. The first is that CNP has a higher cellular uptake rate than Cur. The second factor is that CNP's self-assembly property may enhance its binding affinity to drug targets. Both of these factors work together to contribute to CNP's stronger pharmacological efficacy. Similarly, as shown in Figure 6B, H_2O_2 treatment caused a significant decline in the relative cell growth rate, which dropped to 29.41 ± 1.75%. Following the addition of either Cur or CNP, the relative cell growth rate increased significantly. Consistent with observations in the CORT model, CNP showed stronger biological activity than Cur when administered at the same concentration.

In vitro Anti-Inflammatory Activity Study

Numerous studies have shown that the occurrence and development of depression are closely associated with the regulation of neuroinflammation. As one of the most critical cell types for regulating immune inflammation in CNS, microglia can release a series of pro-inflammatory cytokines. These include IL-1β, IL-6, and TNF-α. These cytokines contribute to the establishment of a chronic inflammatory environment in the brain. This environment then leads to the massive accumulation of neurotoxic substances such as NO and ROS. Ultimately, this accumulation causes neuronal damage and compromises synaptic function.[58] As a pro-inflammatory agent, LPS can significantly upregulate the expression of IL-6 mRNA in the brain and induce depressive-like behaviors. Developing antidepressant agents by modulating neuroinflammation is therefore a highly promising strategy.[59] For this reason, we used the LPS-induced BV2 microglial stress model to evaluate the effects of CNP. As shown in Figure 7A, following LPS treatment, NO release in the model group increased by approximately 3-fold. After treatment with Cur or CNP, this upward trend in NO release was significantly reversed. Notably, compared with the Cur-treated group, the CNP group exerted a stronger inhibitory effect on NO release at the corresponding drug concentration. Similar to its inhibitory effect on NO release, CNP also modulated ROS levels. This observation is clearly supported by Figure 7B and C. Following LPS treatment, the ROS fluorescence intensity in cells of the model group was significantly higher than that in cells of the blank control group. After CNP treatment, the ROS fluorescence intensity was significantly

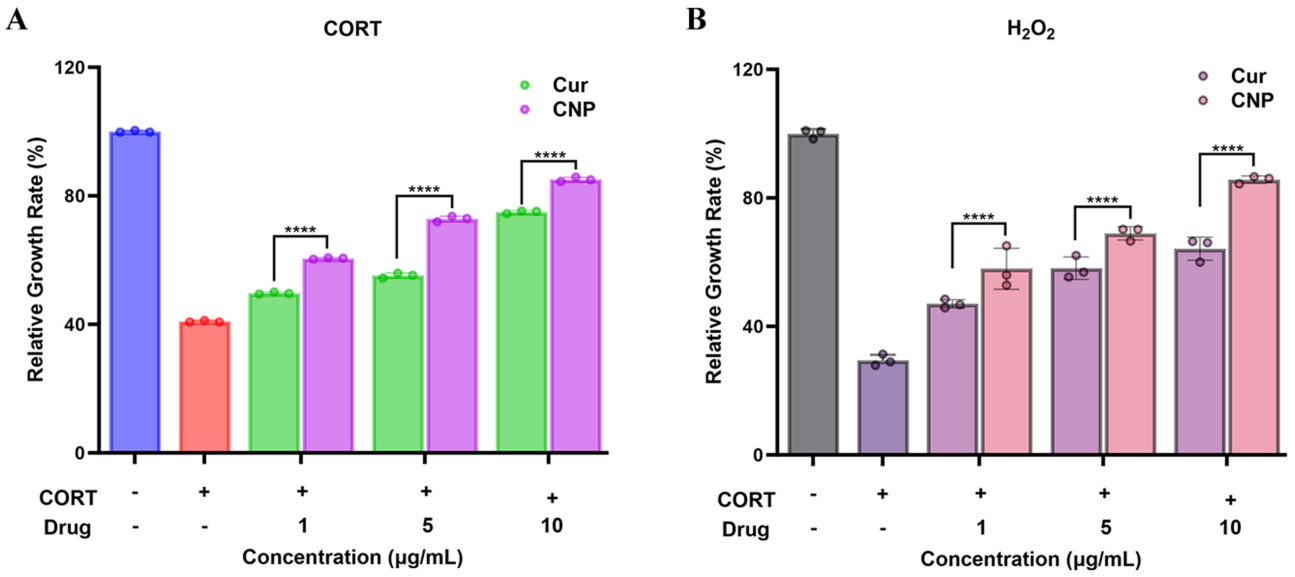

Figure 6 CNP exhibit an enhanced neuroprotective effect. (**A**) Viability recovery effect of Cur and CNP at gradient concentrations on BV2 cells after injury induced by CORT. (**B**) Viability recovery effect of Cur and CNP at gradient concentrations on BV2 cells after injury induced by H_2O_2. ($\bar{x} \pm s$, n = 3).

 https://doi.org/10.2147/IJN.S611765

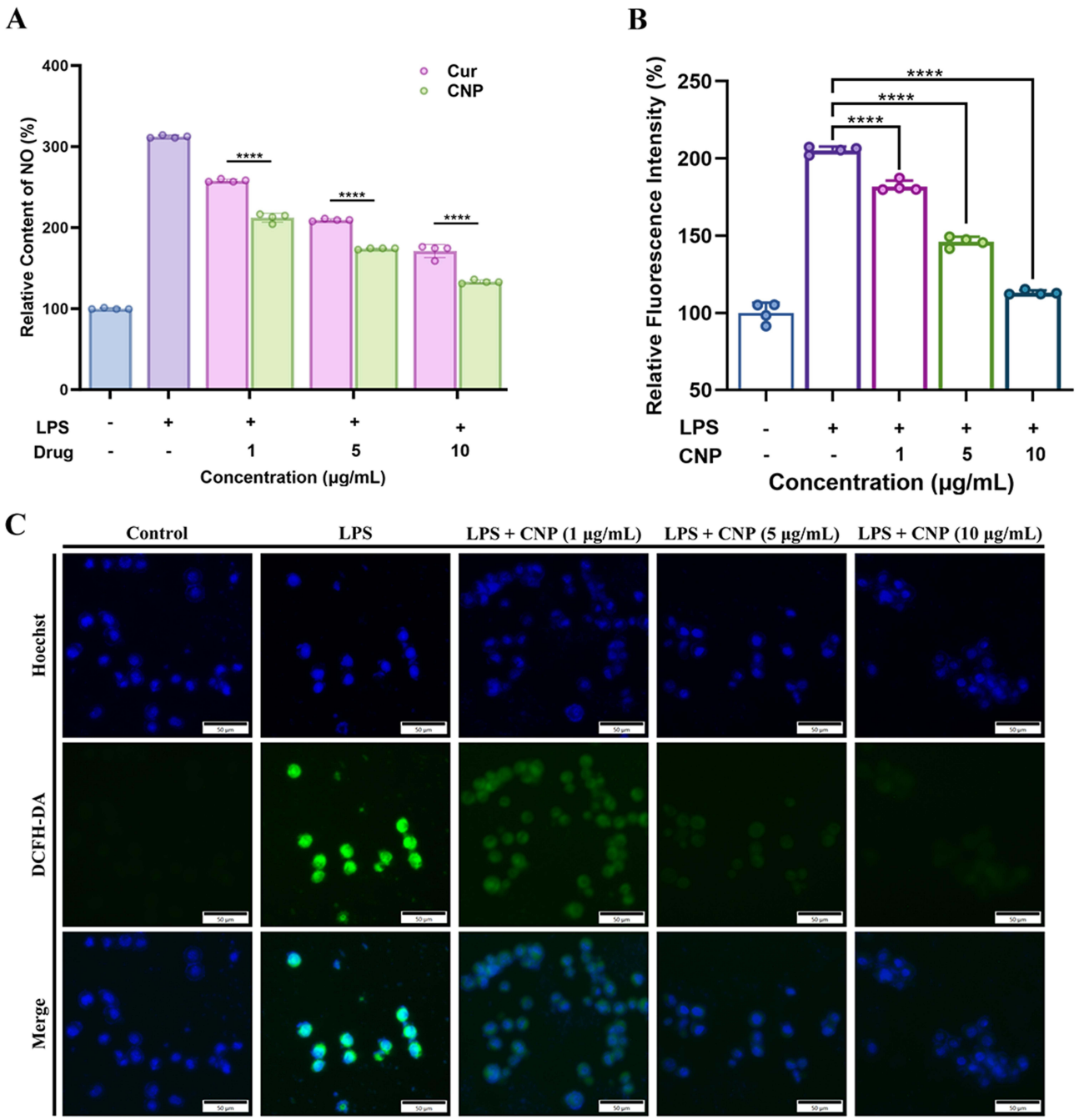

Figure 7 CNP inhibits LPS-induced microglial cytotoxic substances release. (**A**) Inhibition of NO release from BV2 cells by Cur and CNP at gradient concentrations after stress induction by LPS. (**B**) Inhibition of ROS release from BV2 cells by Cur and CNP at gradient concentrations after stress induction by LPS. (**C**) Fluorescence images demonstrate CNP-mediated inhibition of ROS production. ($\bar{x} \pm s$, n = 4).

reduced and exhibited a concentration-dependent pattern. As the CNP concentration increased, the inhibitory effect on ROS became stronger. These observations were further validated by the quantitative results presented in Figure 7B.

In vivo Antidepressant Effect

Following preparative characterization and preliminary in vitro activity assessment confirming CNP's potent antidepressant potential, we further evaluated CNP's in vivo antidepressant efficacy using the CUMS-induced depression model. Fluoxetine (Flu), a first-line clinical drug for depression treatment, served as the positive control. As presented in

https://doi.org/10.2147/IJN.S611765

Figure 8A–C, in the open field test (OFT), compared with the blank control group, CUMS-induced depressed mice exhibited significantly shortened total travel distance (2090.82 ± 165.27 cm vs 934.87 ± 170.16 cm, $P < 0.01$). Similarly, their central zone travel distance was also markedly reduced (134.06 ± 22.62 cm vs 10.80 ± 9.44 cm). Flu intervention significantly enhanced the locomotor activity of depressed mice. This was evidenced by notable increases in both total travel distance (1557.24 ± 136.54 cm) and central zone travel distance (91.91 ± 18.04 cm). This ameliorative effect was further enhanced following CNP administration and exhibited a concentration-dependent pattern with increasing CNP dosage. The low-dose CNP group showed superior improvement compared with the Flu group. Mice in the high-dose CNP group achieved a central zone travel distance of 120.66 ± 16.66 cm, which showed no significant difference from the blank control group. Subsequently, we assessed the mice's performance in the forced swim test (FST). The FST reflects the mice's will to survive. Depressed mice typically show reduced struggle motivation, manifested as prolonged immobility time. Test results are presented in Figure 8D. Mice in the CUMS group exhibited an immobility time of 206.07 ± 23.17 s. Flu, low-dose CNP and high-dose CNP all significantly reversed the immobility phenotype of depressed mice in this test. Among these, the high-dose CNP group exerted the strongest effect, shortening the immobility time to 97.92 ± 26.25 s. We also evaluated the mice's depressive-like behaviors using the sucrose preference test (SPT), with results shown in Figure 8E. The model group displayed comparable consumption of sucrose solution and plain water, resulting in a sucrose preference rate of 52.95 ± 4.98%. After drug intervention, all treatment groups showed varying degrees of recovery, and no significant differences were observed among these three groups. Collectively, the behavioral test results demonstrate that in CUMS-induced depressed mice, CNP administered at 20 mg/kg exerted a more potent antidepressant effect than the clinical first-line drug Flu.

Limitation

In the present study, we adopted the classic CUMS model, which represents the most widely accepted and authoritative paradigm for studying depression and evaluating the antidepressant efficacy of nanomedicines, and it has been extensively applied in most available studies to assess antidepressant therapeutic effects. Although the CUMS model exhibits favorable stability and representativeness and can effectively mimic the core symptoms of depression, it still has certain limitations. First, a single CUMS model cannot fully recapitulate the heterogeneous characteristics of human depression, which may lead to certain deviations in the clinical translation of research conclusions. Second, only the CUMS model was used in this study, and cross-validation with other depression models (such as the chronic social defeat stress model and LPS-induced depressive inflammatory model) was not performed. In addition, detection of a broader range of neuro-molecular mechanism-related indicators would more comprehensively reveal the complete molecular pathway underlying the antidepressant action of CNP. Although our study has verified the promising antidepressant effect of intranasal curcumin nanoparticles in animal models, the potential side effects and biosafety remain to be further clarified. For future clinical translation, intranasal administration of nanoparticles may bring putative adverse effects, including nasal mucosal dryness, local irritation, mild inflammatory reaction, and possible residual accumulation of nanocarriers in the nasal cavity and olfactory pathway. Therefore, comprehensive mucosal compatibility, acute and chronic toxicity tests, as well as in vivo biodistribution safety evaluation are required in subsequent studies to ensure the clinical applicability and safety of this nasal nano-formulation. Finally, this study only focused on the standalone antidepressant effect of curcumin nanoparticles and did not explore their application as adjuvant therapy in combination with clinically used antidepressants. Verifying the synergistic or complementary effects of curcumin nanoparticles combined with these clinical drugs, and exploring the optimal dose ratio, administration route and potential interaction mechanism of the combined administration strategy, will provide more comprehensive preclinical evidence for their clinical application as adjuvant therapy for depression and further improve the clinical translational value of curcumin nanoparticles.

Conclusion

In this study, lipid-based nanoparticles (CNP) with enhanced brain delivery efficiency were fabricated via the self-assembly of Cur, followed by encapsulation within lipids and modification with borneol. After systematic structural characterization of CNP via techniques such as DSC, XRD, and TEM, cellular uptake experiments, evaluation of multiple in vitro antidepressant models, and in vivo studies using the CUMS-induced depressive mouse model collectively demonstrated that CNP exhibits enhanced brain delivery efficiency, favorable biocompatibility, and potent antidepressant effects. In general, this work

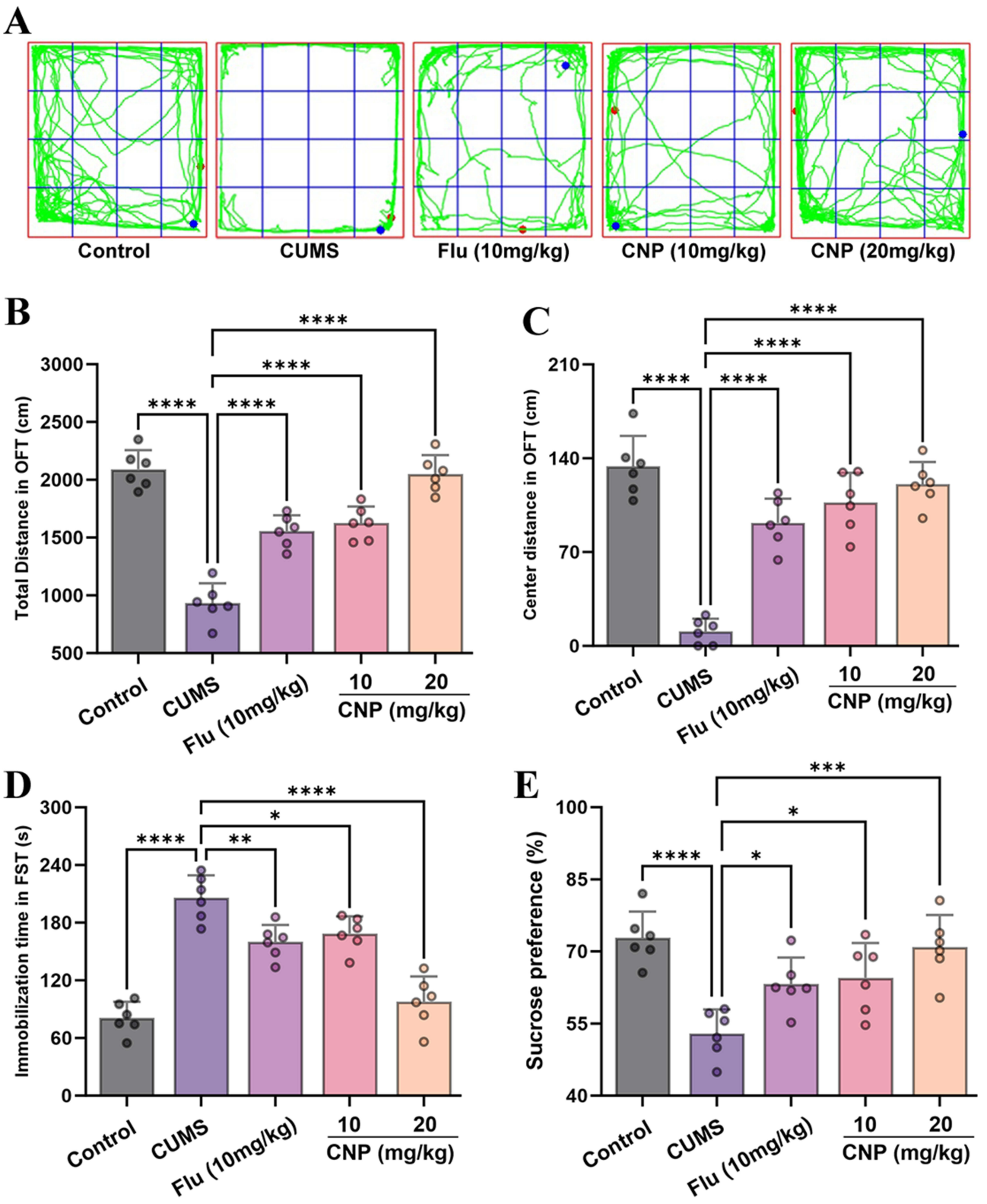

Figure 8 Effects of CNP on depressive-like behaviors in CUMS-induced depressed mice. (**A**) The representative movement trajectory map of mice in each group within the open field test chamber. (**B**) The total movement distance of mice in each group in the open field test chamber. (**C**) The total movement distance of mice in each group within the central area of the open field test chamber. (**D**) The immobility time of mice in each group during the forced swim test. (**E**) The sucrose preference values of mice in each group from the sucrose preference test. **P* < 0.05, ***P* < 0.01, ****P* < 0.001. (x ± s, n = 6).

https://doi.org/10.2147/IJN.S611765

presents a simple and effective strategy for constructing a lipid-based nanodelivery system for pure curcumin nanoparticles. Importantly, intranasally administered CNP shows strong potential as a brain-targeted antidepressant, offering a novel and promising platform for enhancing the brain delivery of therapeutics for MDD. More importantly, the potent antidepressant activity of intranasally administered CNP highlights its great potential as a safe and effective alternative for the clinical management of MDD. This nanodelivery strategy offers a promising and translatable avenue for the development of brain-targeted therapeutics, not only for MDD but also potentially for other central nervous system disorders characterized by impaired drug delivery to the brain. Therefore, the present study provides valuable insights and a reliable technical foundation for accelerating the clinical translation of novel nanomedicines for neuropsychiatric diseases.

Abbreviations

BBB, Blood-brain barrier; Bor, Borneol; CNS, Central nervous system; CORT, Corticosterone; CUMS, Chronic unpredictable mild stress; Cur, Curcumin; DSC, Differential scanning calorimeter; EE, Encapsulation efficiency; Flu, Fluoxetine; FST, Forced swim test; HE, Hematoxylin and eosin; HPA, Hypothalamic-pituitary-adrenal; HPLC, High-performance liquid chromatography; HSPC, Hydrogenated soybean phospholipids; H_2O_2, Hydrogen peroxide; LE, Loading efficiency; LPS, Lipopolysaccharide; MDD, Major depressive disorder; OD, Optical density; OFT, Open field test; ROS, Reactive oxygen species; SPT, Sucrose preference test; TEM, Transmission electron microscopy; XRD, X-ray diffraction.

Data Sharing Statement

The data presented in this study are available on request from the corresponding author.

Ethics Approval and Consent to Participate

The animal studies were done in compliance with the regulations and guidelines of laboratory animal welfare and ethics committee of Chongqing University Central Hospital (NO.2502002) and adhered to the ARRIVE guidelines. The animal license number is SCXK (Beijing) 2024-0001.

Author Contributions

All authors made a significant contribution to the work reported, whether that is in the conception, study design, execution, acquisition of data, analysis and interpretation, or in all these areas; took part in drafting, revising or critically reviewing the article; gave final approval of the version to be published; have agreed on the journal to which the article has been submitted; and agree to be accountable for all aspects of the work.

Funding

This study was supported by the Chongqing medical scientific research project (Joint project of Chongqing Health Commission and Science and Technology Bureau, No.2025QNXM019), the Traditional Chinese Medicine Research Project of Chongqing Municipal Health Commission (Grant No.2025ZYQN018), the Chongqing Clinical Pharmacy Key Specilties Construction Project, and the Yibin Science and Technology Plan Project (No.2025MZ008), the Sichuan Provincial Hospital Association Special Research Fund for Young Pharmacists (No. YP2202402).

Disclosure

The authors declare no conflicts of interest in this work.

References

1. Chan JKN, Solmi M, Lo HKY, et al. All-cause and cause-specific mortality in people with depression: a large-scale systematic review and meta-analysis of relative risk and aggravating or attenuating factors, including antidepressant treatment. *World Psychiatry*. 2025;24(3):404–421. doi:10.1002/wps.21354
2. Wang X, Su Y, Liu Q, et al. Unveiling diverse clinical symptom patterns and neural activity profiles in major depressive disorder subtypes. *EBioMedicine*. 2025;116:105756. doi:10.1016/j.ebiom.2025.105756
3. Lagerberg T, Matthews AA, Zhu N, Fazel S, Carrero -J-J, Chang Z. Effect of selective serotonin reuptake inhibitor treatment following diagnosis of depression on suicidal behaviour risk: a target trial emulation. *Neuropsychopharmacology*. 2023;48(12):1760–1768. doi:10.1038/s41386-023-01676-3

4. Protti M, Mandrioli R, Marasca C, Cavalli A, Serretti A, Mercolini L. New-generation, non-SSRI antidepressants: drug-drug interactions and therapeutic drug monitoring. Part 2: naSSAs, NRIs, SNDRIs, MASSAs, NDRI s, and others. *Med Res Rev*. 2020;40(5):1794–1832. doi:10.1002/med.21671
5. Cardona-Acosta AM, Parise LF, Bolaños-Guzmán CA, Parise EM. Prophylactic Ketamine: current knowledge and future directions. *Biol Psychiatry*. 2025;98(7):517–530.
6. Chen T, Cheng L, Ma J, et al. Molecular mechanisms of rapid-acting antidepressants: new perspectives for developing antidepressants. *Pharmacol Res*. 2023;194:106837. doi:10.1016/j.phrs.2023.106837
7. Richardson E, Patterson R, Meltzer-Brody S, McClure R, Tow A. Transformative therapies for depression: postpartum depression, major depressive disorder, and treatment-resistant depression. *Annu Rev Med*. 2025;76(1):81–93. doi:10.1146/annurev-med-050423-095712
8. Mojtabai R, Amin-Esmaeili M, Spivak S, Olfson M. Remission and treatment augmentation of depression in the United States. 2021. 82 (6):21m13988.
9. Zhao R, Wang J, Chung SK, Xu B. New insights into anti-depression effects of bioactive phytochemicals. *Pharmacol Res*. 2025;212:107566. doi:10.1016/j.phrs.2024.107566
10. Zeng J, Wang Z, Zhang X, et al. Exploring the neuroplasticity hypothesis in depression: the role of traditional Chinese herbal medicine. *Phytomedicine*. 2025;143:156927. doi:10.1016/j.phymed.2025.156927
11. Wang Y-S, Shen C-Y, Jiang J-G. Antidepressant active ingredients from herbs and nutraceuticals used in TCM: pharmacological mechanisms and prospects for drug discovery. *Pharmacol Res*. 2019;150:104520. doi:10.1016/j.phrs.2019.104520
12. Figueiredo Godoy AC, Frota FF, Araújo LP, et al. Neuroinflammation and Natural Antidepressants: balancing Fire with Flora. *Biomedicines*. 2025;13(5):1129. doi:10.3390/biomedicines13051129
13. Merino JJ, Parmigiani-Cabaña JM, Parmigiani-Izquierdo JM, Fernández-García R, Cabaña-Muñoz ME. Decreased systemic Monocyte Colony Protein-1 (MCP-1) levels and reduced sCD14 levels in curcumin-treated patients with moderate anxiety: a pilot study. *Antioxidants*. 2024. 13 (9):1052.
14. Cheng Y-C, Huang W-L, Chen W-Y, Huang Y-C, Kuo P-H, Tu Y-K. Comparative efficacy and tolerability of nutraceuticals for depressive disorder: a systematic review and network meta-analysis. *Psychol Med*. 2025;55:e134. doi:10.1017/S0033291725000996
15. Sanmukhani J, Satodia V, Trivedi J, et al. Efficacy and safety of curcumin in major depressive disorder: a randomized controlled trial. *Phytother Res*. 2014;28(4):579–585. doi:10.1002/ptr.5025
16. Fusar-Poli L, Vozza L, Gabbiadini A, et al. Curcumin for depression: a meta-analysis. *Crit Rev Food Sci Nutr*. 2020;60(15):2643–2653. doi:10.1080/10408398.2019.1653260
17. Lopresti AL. Potential role of curcumin for the treatment of major depressive disorder. *CNS Drugs*. 2022;36(2):123–141. doi:10.1007/s40263-022-00901-9
18. Radbakhsh S, Butler AE, Moallem SA, Sahebkar A. The effects of curcumin on brain-derived neurotrophic factor expression in neurodegenerative disorders. *Curr Med Chemist*. 2023. 31(36):5937–52.
19. Jing G, Meng F, Zhe X, Ke Z, Peng Z. Mechanistic insights into the anti-depressant effect of curcumin based on network pharmacology and experimental validation. *Naunyn-Schmiedeberg's Arch Pharmacol*. 2023;397(1):583–598.
20. Anand P, Kunnumakkara AB, Newman RA, Aggarwal BB. Bioavailability of curcumin: problems and promises. *Mol Pharm*. 2007;4(6):807–818. doi:10.1021/mp700113r
21. Wang Z, Yang L. Natural-product-based, carrier-free, noncovalent nanoparticles for tumor chemo-photodynamic combination therapy. *Pharmacol Res*. 2024;203:107150.
22. Zhao DJ, Tian C, Cheng M, et al. Carrier-free quercetin nanomedicine blocks NLRP3 deubiquitination and TXNIP recruitment for Parkinson's disease therapy. *Chem Eng J*. 2023;464:142697.
23. Yao Y, Xu Z, Ding H, et al. Carrier-free nanoparticles-new strategy of improving druggability of natural products. *J Nanobiotechnology*. 2025;23 (1):108. doi:10.1186/s12951-025-03146-y
24. Yang W, Shi Y, Zhang Y, et al. Intranasal carrier-free nanomodulator addresses both symptomatology and etiology of alzheimer's disease by restoring neuron plasticity and reprogramming lesion microenvironment. *ACS Nano*. 2024;18(43):29779–29793. doi:10.1021/acsnano.4c09449
25. Reker D, Rybakova Y, Kirtane AR, et al. Computationally guided high-throughput design of self-assembling drug nanoparticles. *Nat Nanotechnol*. 2021;16(6):725–733. doi:10.1038/s41565-021-00870-y
26. An J, Zhang Z, Zhang J, Zhang L, Liang G. Research progress in tumor therapy of carrier-free nanodrug. *Biomed Pharmacother*. 2024;178:117258. doi:10.1016/j.biopha.2024.117258
27. Quinlan JA, Inglut CT, Srivastava P, et al. Carrier-free, amorphous verteporfin nanodrug for enhanced photodynamic cancer therapy and brain drug delivery. *Adv Sci*. 2024;11(17):e2302872. doi:10.1002/advs.202302872
28. Feng Q, Zhang X, Zhao X, et al. Intranasal delivery of pure nanodrug loaded liposomes for alzheimer's disease treatment by efficiently regulating microglial polarization. *Small*. 2024;20(50):e2405781. doi:10.1002/smll.202405781
29. Jinfeng Z, Weidong N, Rui C, et al. Green mass production of pure nanodrugs via an ice-template-assisted strategy. *Nano Lett*. 2018;19(2):658–65.
30. Mei H, Cai S, Huang D, Gao H, Cao J, He B. Carrier-free nanodrugs with efficient drug delivery and release for cancer therapy: from intrinsic physicochemical properties to external modification. *Bioact Mater*. 2022;8:220–240. doi:10.1016/j.bioactmat.2021.06.035
31. Fang F, Chen X. Carrier-Free Nanodrugs: from Bench to Bedside. *ACS Nano*. 2024;18(35):23827–23841. doi:10.1021/acsnano.4c09027
32. Xia D, He Y, Li Q, et al. Transport mechanism of lipid covered saquinavir pure drug nanoparticles in intestinal epithelium. *J Control Release*. 2018;269:159–170. doi:10.1016/j.jconrel.2017.11.012
33. Drath I, Richter F, Feja M. Nose-to-brain drug delivery: from bench to bedside. *Transl Neurodegener*. 2025;14(1):23. doi:10.1186/s40035-025-00481-w
34. Patel M, Minglani VV, Vaddadi H, et al. Advancements in nanotherapeutics for the treatment of depression via intranasal pathway: a review. *Int J Nanomed*. 2025;20:7323–7342. doi:10.2147/IJN.S525759
35. Liu L, Liu M, Xiu J, et al. Stimuli-responsive nanoparticles delivered by a nasal-brain pathway alleviate depression-like behavior through extensively scavenging ROS. *Acta Biomater*. 2023;171:451–465.
36. Upadhyay R, Ghosh P, Desavathu M. Advancement in the nose-to-brain drug delivery of FDA-approved drugs for the better management of depression and psychiatric disorders. *Int J Pharm*. 2024;667(Pt B):124866.

37. Can Karaca A, Rezaei A, Qamar M, Assadpour E, Esatbeyoglu T, Jafari SM. Lipid-based nanodelivery systems of curcumin: recent advances, approaches, and applications. *Food Chem*. 2025;463(Pt 2):141193. doi:10.1016/j.foodchem.2024.141193
38. Yan Y, Sun Y. Advancing cancer therapy: nanomaterial-based encapsulation strategies for enhanced delivery and efficacy of curcumin. *Mater Today Bio*. 2025;33:101963. doi:10.1016/j.mtbio.2025.101963
39. Lagoa R, Rajan L, Violante C, et al. Application of curcuminoids in inflammatory, neurodegenerative and aging conditions - Pharmacological potential and bioengineering approaches to improve efficiency. *Biotechnol Adv*. 2025;82:108568.
40. Rubab S, Naeem K, Rana I, et al. Enhanced neuroprotective and antidepressant activity of curcumin-loaded nanostructured lipid carriers in lipopolysaccharide-induced depression and anxiety rat model. *Int J Pharm*. 2021;603:120670. doi:10.1016/j.ijpharm.2021.120670
41. Wang Y, Ma X, Wang X, et al. Traditional Chinese medicine borneol-based polymeric micelles intracerebral drug delivery system for precisely pathogenesis-adaptive treatment of ischemic stroke. *Adv Sci*. 2025;12(9):e2410889. doi:10.1002/advs.202410889
42. Hu X, Yan Y, Liu W, et al. Advances and perspectives on pharmacological activities and mechanisms of the monoterpene borneol. *Phytomedicine*. 2024;132:155848. doi:10.1016/j.phymed.2024.155848
43. Liu S, Long Y, Yu S, et al. Borneol in cardio-cerebrovascular diseases: pharmacological actions, mechanisms, and therapeutics. *Pharmacol Res*. 2021;169:105627. doi:10.1016/j.phrs.2021.105627
44. Xia C, Hu C, Xu R, et al. An efficient brain delivery system co-loaded with multiple components of Salvia miltiorrhiza for synergistic treatment of ischemic stroke. *Mater Today Bio*. 2025;34:102102. doi:10.1016/j.mtbio.2025.102102
45. Luo Q, Yang J, Yang M, et al. Utilization of nanotechnology to surmount the blood-brain barrier in disorders of the central nervous system. *Mater Today Bio*. 2025;31:101457. doi:10.1016/j.mtbio.2025.101457
46. Kan G, Chen L, Zhang W, Bian Q, Wang X, Zhong J. Recent advances in the development and application of curcumin-loaded micro/nanocarriers in food research. *Adv Colloid Interface Sci*. 2025;335:103333. doi:10.1016/j.cis.2024.103333
47. Filho CB, Jesse CR, Donato F, et al. Neurochemical factors associated with the antidepressant-like effect of flavonoid chrysin in chronically stressed mice. *Eur J Pharmacol*. 2016;791:284–296. doi:10.1016/j.ejphar.2016.09.005
48. Fan Y, Marioli M, Zhang K. Analytical characterization of liposomes and other lipid nanoparticles for drug delivery. *J Pharm Biomed Anal*. 2021;192:113642. doi:10.1016/j.jpba.2020.113642
49. Li Q, Lianghao Y, Shijie G, et al. Self-assembled nanodrug delivery systems for anti-cancer drugs from traditional Chinese medicine. *Biomater Sci*. 2024;12(7):1662–1692. doi:10.1039/D3BM01451G
50. Liu J, Wang T, Dong J, Lu Y. The blood-brain barriers: novel nanocarriers for central nervous system diseases. *J Nanobiotechnology*. 2025;23(1):146.
51. Zhaoyu L, Jingxun C, Mingkun X, et al. Engineered multi-domain lipid nanoparticles for targeted delivery. 2025;54(12):5961–94.
52. O'Brien Laramy M, Foley DA, Pak RH, et al. Chemistry, manufacturing and controls strategies for using novel excipients in lipid nanoparticles. *Nat Nanotechnol*. 2025;20(3):331–344. doi:10.1038/s41565-024-01833-9
53. Tong Z, Jie X, Chen Z, et al. Borneol and lactoferrin dual-modified crocetin-loaded nanoliposomes enhance neuroprotection in HT22 cells and brain targeting in mice. *Eur J Med Chem*. 2024;276:116674. doi:10.1016/j.ejmech.2024.116674
54. Murray F, Smith DW, Hutson PH. Chronic low dose corticosterone exposure decreased hippocampal cell proliferation, volume and induced anxiety and depression like behaviours in mice. *Eur J Pharmacol*. 2008;583(1):115–127.
55. Wang G, Cao L, Li S, et al. Corticosterone impairs hippocampal neurogenesis and behaviors through p21-mediated ROS accumulation. *Biomolecules*. 2024;14(3):268. doi:10.3390/biom14030268
56. Salim S. Oxidative stress and psychological disorders. *Curr Neuropharmacol*. 2014;12(2):140–147. doi:10.2174/1570159X11666131120230309
57. Ding Q, Li D, Zhang X, et al. Restoring the Redox and Norepinephrine Homeostasis in Mouse Brains Promotes an Antidepressant Response. *J Am Chem Soc*. 2025;147(13):11239–11249. doi:10.1021/jacs.4c18046
58. Kim Y-K, Na K-S, Myint A-M, Leonard BE. The role of pro-inflammatory cytokines in neuroinflammation, neurogenesis and the neuroendocrine system in major depression. *Prog Neuropsychopharmacol Biol Psychiatry*. 2016;64:277–284.
59. Liu D, Wang Z, Liu S, Wang F, Zhao S, Hao A. Anti-inflammatory effects of fluoxetine in lipopolysaccharide(LPS)-stimulated microglial cells. *Neuropharmacology*. 2011;61(4):592–599.